Applied Catalysis B: Environmental 132–133 (2013) 511–518

Contents lists available at SciVerse ScienceDirect

Applied Catalysis B: Environmental

journal homepage: www.elsevier.com/locate/apcatb

# Activity controlling factors for low-temperature oxidation of CO over supported Pd catalysts

Atsushi Satsuma[a,b,*], Kaoru Osaki[a], Masatoshi Yanagihara[a], Junya Ohyama[a,b], Kenichi Shimizu[b,c]

[a] Graduate School of Engineering, Nagoya University, Nagoya 464-8603, Japan
[b] Unit of Elements Strategy Initiative for Catalysts & Batteries, Kyoto University, Kyoto 615-8530, Japan
[c] Catalysis Research Center, Hokkaido University, Sapporo 001-0021, Japan

ARTICLE INFO

*Article history:*
Received 31 August 2012
Received in revised form
11 December 2012
Accepted 15 December 2012
Available online 25 December 2012

*Keywords:*
Pd
Support effect
CO oxidation
Oxygen storage capacity
Activity-controlling factor

ABSTRACT

The effect of supports ($CeO_2$, $TiO_2$, $Al_2O_3$, $ZrO_2$, and $SiO_2$) on CO oxidation over Pd catalysts at low temperatures was investigated, and activity-controlling factors were discussed. The light-off temperature was in the order of $Pd/CeO_2 < Pd/TiO_2 < Pd/Al_2O_3 < Pd/ZrO_2 \leq Pd/SiO_2$ which was fairly in agreement with the reduction temperature of supported Pd to metallic species in CO-Temperature programmed reduction (CO-TPR) profile. The result indicates that higher reducibility of supported Pd to metallic species is one of the activity-controlling factors for the oxidation activity. The activation of oxygen on metal oxide support is suggested to be another factor for the low temperature oxidation. Actually, in situ IR measurement revealed that the oxidation of CO proceeds on $Pd/CeO_2$ and $Pd/TiO_2$ even under nearly 100% coverage of CO over Pd, though $Pd/Al_2O_3$ showed CO oxidation activity below 50% coverage of CO. The supports having oxygen storage property, $CeO_2$ and $TiO_2$, contribute to the oxygen activation to proceed CO oxidation irrespective of self-poisoning of metallic Pd surface by adsorbed CO. It was concluded that both of the following two factors are essential for CO oxidation at low temperature: (1) formation of metallic Pd and (2) oxygen storage property of metal oxide support.



## 1. Introduction

Supported Pd catalyst is an active component for pollutant control, i.e., total oxidation of CO, hydrocarbons especially methane, volatile organic compounds (VOCs), and also an essential component for an automobile three-way catalyst (TWC). Promotion of catalytic activity at lower temperatures is strongly desired to achieve complete reduction of pollutants. For example, the wider use of better fuel economy cars, of which the exhaust gas temperature is lower than that of ordinary cars, is promoting demand for the higher catalytic activity at lower temperatures. As one of the effective strategy for the enhancement of catalytic activity of supported Pd catalysts, the importance of metal oxide supports is well recognized, and various papers have been reported on the effect of supports on the total oxidation of methane [1–13], other hydrocarbons [14–18], and CO [19–33].

$CeO_2$ and $CeO_2$-based metal oxides often show significant role in the promotion of the activity of supported Pd. One of the merits of $CeO_2$-based supports is higher dispersion of Pd species [19,29,33]. Gulyaev et al. [33] reported that the use of $CeO_2$ as a support resulted in the formation of solid solutions of $Pd_xCe_{1-x}O_{2-\delta}$ and palladium clusters with highly dispersed state. The similar self-dispersion can be observed in perovskite-based catalyst ($LaFe_{0.57}Co_{0.38}Pd_{0.05}O_3$) which shows an excellent thermal-durability [19,20,34]. In contrast, there is the case that lower dispersion of Pd is more preferable for the higher activity depending on the pretreatment conditions [17,18]. This is because highly dispersed Pd particles are easily oxidized to less active PdO or ionic $Pd^{2+}$ under the reaction atmosphere, which results in the decrease in active metallic Pd and thus lower catalytic activity. Kim et al. also pointed out the higher importance of the formation of metallic Pd than the dispersion of Pd [17]. Depending on the reaction conditions, the metallic state of Pd is more essential for the catalytic activity than Pd dispersion.

There are still some discussions on the oxidation state of active Pd species. In the methane oxidation, the important role of the Pd/PdO transformation process on the catalytic activity is well recognized. Yoshida et al. investigated the effect of $CH_4/O_2$ concentrations on the methane oxidation over supported Pd [8]. The methane conversion strongly depends on the $CH_4/O_2$ ratio, and the maximum activity was observed when Pd metal and PdO*x* are co-presence on the surface. Castellazzi et al. [12] clarified that reduction–oxidation cycles of $Pd/Al_2O_3$ resulted in the increase of catalytic activity for methane oxidation. Specchia et al.

* Corresponding author at: Nagoya University, Graduate School of Engineering, Furo-cho, Chikusa-ku, Nagoya, Aichi, 464-8603 Japan. Tel.: +81 52 789 4608; fax: +81 52 789 3193.
*E-mail address:* satsuma@apchem.nagoya-u.ac.jp (A. Satsuma).

0926-3373/$ – see front matter © 2012 Elsevier B.V. All rights reserved.
http://dx.doi.org/10.1016/j.apcatb.2012.12.025

[35,36] presented that the high activity for methane oxidation over Pd/$CeO_2$-$ZrO_2$ and Pd/La-Mn-Zr-O catalysts is due to the synergies between partly oxidized small Pd metal particles as an activation site of methane and dispersed Pd oxide species as an oxygen provider. Schalow et al. [37] investigated a Pd/$Fe_3O_4$ model catalyst using molecular beam, time resolved IR reflection absorption spectroscopy, and photoelectron spectroscopy. The oxidation of the catalyst results in the formation of Pd oxide species as a thin layer at the particle/support interface, stabilized by the iron-oxide support. The oxygen is released upon decomposition of Pd oxide and migrates back onto the metallic part of the Pd surface, thus the Pd interface oxide layer acts as an oxygen reservoir. The role of oxidized Pd is also supported by other groups [1,8,14,31].

On the other hand, metallic Pd phase is also assigned to be the active phase [33,38–40]. Lyubovsky and Pfefferle [38] emphasized the higher activity of metallic Pd than oxidized one on the basis of a sharp increase in the methane conversion by in situ hydrogen reduction and lower activity at higher oxygen concentrations. Jin et al. presented that higher calcination temperature of Pd/$Ce_{0.2}Y_{0.8}O_{2-\delta}$ showed higher catalytic activity because of the decrease in the average oxidation state of Pd, thus lower oxidation state is preferable for the oxidation activity [39]. As can be seen in the literature, the apparent active phase of Pd strongly depends on catalysts and reaction conditions, such as metal oxide support, reaction temperature, reactants, oxygen concentrations, and so on. Therefore, attention on reaction conditions should be paid for the discussions on the active phase of Pd.

Oxygen storage and release properties of supports are also pointed out to be a critical factor for the catalytic activity of Pd-supported catalysts at low temperatures. Several papers have been demonstrated that suitable design of $CeO_2$-based metal oxide supports, such as $CeO_2$ [41–43], $CeO_2$/$Co_3O_4$ [25,44,45] and $CeO_2$-$TiO_2$ [22,46–48], significantly promote the catalytic activity of CO oxidation. One of the effects of $CeO_2$-based support is attributed to the contribution of lattice oxygen at the interface between metal particle and $CeO_2$ [41]. An iron oxide support also promotes low temperature oxidation. Liu et al. [32] reported that FeO*x*-supported Pd and Pt possess very high activity for low-temperature CO oxidation because of oxygen supply from partly reduced FeO*x* support.

Based on the above literature, catalytic activity of supported Pd catalysts is not derived from a sole factor, but from complicated effects of multiple factors. Therefore, a systematic study should be made to clarify the activity-controlling factors. The aim of this study is a systematic understanding of the activity-controlling factors of supported Pd catalysts. To focus the activity-controlling factors for the low temperature catalytic oxidation, the present study investigated the oxidation of CO because of the lower range of reaction temperature. The profile of Pd was characterized by CO-Temperature programmed reduction, kinetic analysis, and operando analysis by in situ FT/IR connected with CO/$CO_2$ analyzer. The effects of both Pd oxidation state and oxygen storage property were discussed.

## 2. Experimental

### 2.1. Catalyst preparation

Supported Pd catalysts were prepared by a conventional impregnation method using an aqueous palladium nitrate, followed by dryness and calcination in air at 500 °C for 3 h. $CeO_2$ (JRC-CEO-3), $TiO_2$ (JRC-TIO-4), and $ZrO_2$ (JRC-ZRO-1), were supplied from the committee of reference catalyst, Catalysis society of Japan. $Al_2O_3$ was obtained by calcination of boehmite at 900 °C in air for 3 h. $SiO_2$ was supplied from Fuji Silysia Chemical Ltd. (Q-10). The loading amount of Pd was 1 wt%, except 5 wt% Pd/$SiO_2$ used in Section 3.3.

### 2.2. CO oxidation

The catalytic activity was evaluated by CO oxidation using a conventional fixed-bed flow reactor at atmospheric pressure with a 10 mg of catalyst inside a Pyrex glass tube with internal diameter of 4 mm and a total flow rate of 100 N cm$^3$ min$^{-1}$ which corresponds to GHSV = 480,000 h$^{-1}$ [18]. For a continuous flow reaction, a catalyst was at first reduced in a flow of 3%$H_2$/He at 400 °C for 10 min. After the pretreatment, the catalytic run was carried out under a flow of 0.45% CO/10% $O_2$/He. The effluent gas was analyzed by nondispersive infrared (NDIR) CO/$CO_2$ analyzer (Horiba VIA510). The concentrations of CO and $CO_2$ were analyzed during stepwise increase in the reaction temperature, and the steady state CO conversion was measured after 30 min for each temperature.

For a periodic CO–$O_2$ pulse reaction, using the same apparatus for a continuous flow reaction, a 10 mg of catalyst was at first treated at 100 °C in a flow of 0.45% CO/He (100 N cm$^3$ min$^{-1}$) for 5 min, switched to a flow of 10% $O_2$/He for 10 min, and again switched to a flow of 0.45% CO/He for 10 min.

### 2.3. Characterization

Temperature programmed reduction by CO (CO-TPR) was carried out as follows. The supported Pd was oxidized to PdO in a flow of 20%$O_2$/He (100 N cm$^3$ min$^{-1}$) at 400 °C for 10 min. After cooling the sample in a flow of pure He to room temperature, the TPR measurement was carried out in a flow of 0.45%CO/He at a rate of 5 °C min$^{-1}$ up to 400 °C. The effluent gas was analyzed by nondispersive infrared (NDIR) CO/$CO_2$ analyzer (Horiba VIA510).

The dispersion of Pd was estimated by the CO–pulse method [49–51]. A catalyst was at first treated in a flow of $O_2$ at 400 °C for 15 min followed by purge with He for 15 min, and then reduced in a flow of $H_2$ at 400 °C for 15 min followed by purge with He for 15 min. Then the catalyst was cooled in a flow of He, and a series of CO pulses were injected with an interval of 2–3 min until the amount of slipped CO pulses reaches a steady state value. In order to avoid oxidation of CO to $CO_2$ followed by adsorption on $CeO_2$ as carbonate, the sample cell was soaked in a dry ice/ethanol bath and the adsorption of CO was carried out at ca. −70 °C.

The BET specific surface area of the support was measured through $N_2$ adsorption at liquid $N_2$ temperature by using a conventional flow-type adsorption apparatus. The samples were pre-treated at 400 °C in a flow of He for 30 min. XRD patterns were recorded on a Rigaku MiniFlex II/AP diffractometer with Cu Kα radiation. The Pd particle size analysis was carried out by observation using HITACHI H-800 transmission electron microscope operated at 200 kV. For TEM characterization, a sample deposited onto a carbon-coated copper grid (Okenshoji Co. Ltd.). Catalyst was suspended in ethanol and cast by dropping the suspension onto a grid and dried to the solvent at room temperature.

The operando IR measurement was performed using a JASCO FT/IR-6100 equipped with a quartz in situ IR cell [52], which was connected to a conventional flow reaction system upstream and a nondispersive infrared (NDIR) CO/$CO_2$ analyzer (Horiba VIA510) downstream. The sample was pressed into a 20 mg of self-supporting wafer and mounted into the IR cell with $CaF_2$ windows. The spectra were measured by accumulating 15 scans at a resolution of 4 cm$^{-1}$. A reference spectrum of the catalyst wafer after 3%$H_2$/He at 400 °C for 10 min followed by cooling to room temperature in He. The catalyst wafer was then exposed in a flow of 0.45% CO/10% $O_2$/He at a rate of 100 N cm$^3$ min$^{-1}$ with stepwise increase in the reaction temperature. The steady state CO conversion and IR

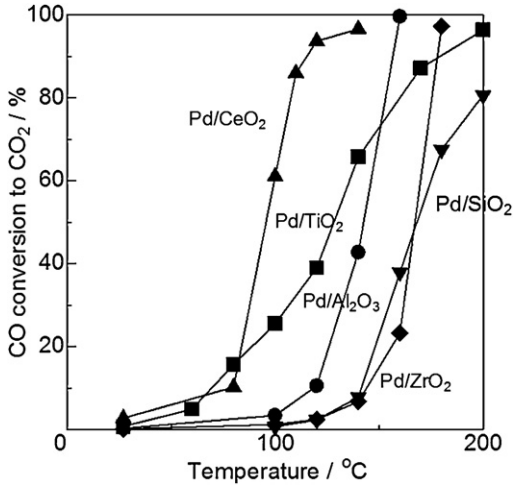


**Fig. 1.** Conversion of CO to $CO_2$ over Pd supported catalysts (Pd 1 wt%) as a function of reaction temperature.

spectrum were measured after 30 min for each temperature, in the same manner of the catalytic runs of CO oxidation.

## 3. Results and discussion

### 3.1. Catalytic activity for CO oxidation

Fig. 1 shows the conversion of CO to $CO_2$ over Pd catalysts supported on $CeO_2$, $TiO_2$, $Al_2O_3$, $ZrO_2$, and $SiO_2$ as a function of temperature. $Pd/CeO_2$ showed the highest activity. The light-off temperature was below 100 °C, and the CO conversion reached to around 100% at 150 °C. The reaction temperature range of $Pd/CeO_2$ was nearly 50 °C lower than that of $Pd/Al_2O_3$. The light-off temperature of $Pd/TiO_2$ was also below 100 °C, but $Pd/TiO_2$ showed lower activity than $Pd/Al_2O_3$ above 150 °C. Comparing the temperature at the CO conversion of 50%, the order of the activity was $Pd/CeO_2 > Pd/TiO_2 > Pd/Al_2O_3 > Pd/ZrO_2 \geq Pd/SiO_2$.

Table 1 shows BET surface area and the dispersion of Pd of the catalysts. The surface areas of $Pd/Al_2O_3$ and $Pd/SiO_2$ were high, those of $Pd/CeO_2$ and $Pd/TiO_2$ were moderate, and that of $Pd/ZrO_2$ was the lowest. The dispersion of Pd was basically proportional to the surface area, however, the dispersions of Pd on $Pd/TiO_2$ was lower than that expected from the surface area. The high activity of $Pd/CeO_2$ and $Pd/TiO_2$ cannot be explained by the dispersion of Pd. Especially, $Pd/TiO_2$ showed the lowest Pd dispersion while the catalytic activity was higher than $Pd/Al_2O_3$ at lower temperatures. The similar results were reported by Kim et al. [17]: Pd catalysts supported on the less specific surface areas ($CeO_2$ and $TiO_2$) showed the higher catalytic activity for propane oxidation. Although it is commonly known that the oxidation activity of Pd cluster would be improved with the increase in Pd cluster size, the highest activity of $Pd/CeO_2$ cannot be rationalized with this knowledge. The results indicate that the priority of Pd dispersion is not high as an activity-controlling factor of Pd supported catalysts. Then, the effect of oxidation state of Pd was examined in the next section.

**Table 1**
BET surface area and dispersion of Pd on a series of supported Pd catalysts (Pd 1 wt%).

| Catalyst | Surface area ($m^2\,g^{-1}$) | Pd dispersion (%) |
|---|---|---|
| $Pd/CeO_2$ | 26 | 25 |
| $Pd/TiO_2$ | 39 | 8.9 |
| $Pd/Al_2O_3$ | 111 | 54 |
| $Pd/ZrO_2$ | 11 | 10 |
| $Pd/SiO_2$ | 101 | 16 |

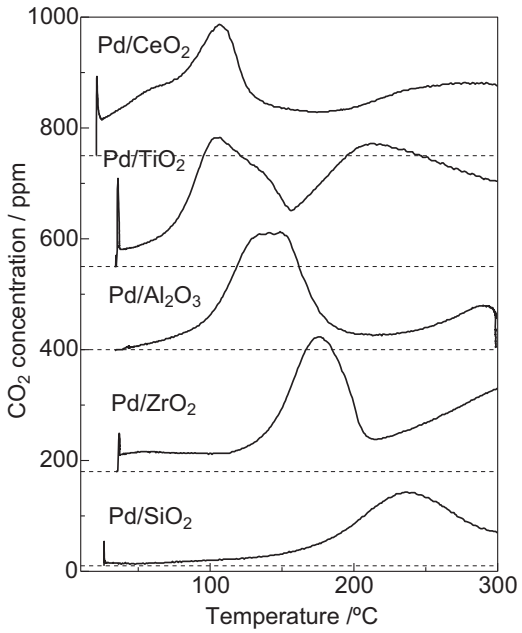


**Fig. 2.** CO-TPR profiles of Pd supported catalysts (Pd 1 wt%).

### 3.2. Oxidation state of Pd

Fig. 2 shows CO-TPR profiles of the supported Pd catalysts. The temperature of the reduction peak and the total amount of produced $CO_2$ are listed in Table 2. Before the TPR measurement, the supported Pd was oxidized to PdO, and the TPR measurement was carried out in 0.45%CO/He without $O_2$. As the simplest case, $Pd/Al_2O_3$ showed a single reduction peak starting from room temperature, showing the reduction maximum at 149 °C. $Pd/ZrO_2$ and $Pd/SiO_2$ also showed single reduction peaks with the maximum at 176 °C, and 236 °C, respectively. The amount of evolved $CO_2$ was 0.10 mmol $g^{-1}$, which is equivalent to the oxygen consumption for the reduction of PdO to Pd. In the case of $Pd/CeO_2$ and $Pd/TiO_2$, the $CO_2$ evolution started at room temperature, the first reduction peak maximum was observed at 106 °C, and then the second peak also appeared above 150 °C. The total $CO_2$ formation exceeded 0.10 mmol $g^{-1}$, indicating oxygen supply from both oxidized Pd and support material.

Comparing the maximum reduction temperature in CO-TPR and the light-off temperature in the activity pattern of CO oxidation, the temperature ranges for CO oxidation are correlated to the reduction of PdO to Pd. The results suggest that the reduction of Pd particles to the metallic state is one of the controlling factors for the activity of CO oxidation, which has been already pointed out in the literature [12,17,18,53]. However, the activity pattern cannot be fully rationalized by CO-TPR. Although PdO on $CeO_2$ and $TiO_2$ was reduced almost the same temperature range, $Pd/CeO_2$ showed higher activity than $Pd/TiO_2$. This mismatch indicates the contribution of the

**Table 2**
$T_{50}$ in CO oxidation and results CO-TPR.

| Catalyst | $T_{50}$ (°C)[a] | CO-TPR | |
|---|---|---|---|
| | | Temperature (°C) | Evolved $CO_2$ (mmol $g^{-1}$)[b] |
| $Pd/CeO_2$ | 97 | 106 | 0.39 |
| $Pd/TiO_2$ | 121 | 106 | 0.16 |
| $Pd/Al_2O_3$ | 143 | 149 | 0.10 |
| $Pd/ZrO_2$ | 167 | 176 | 0.10 |
| $Pd/SiO_2$ | 168 | 236 | 0.11 |

[a] Temperature at which CO conversion is 50%.
[b] The amount of evolved $CO_2$ during the first peak.

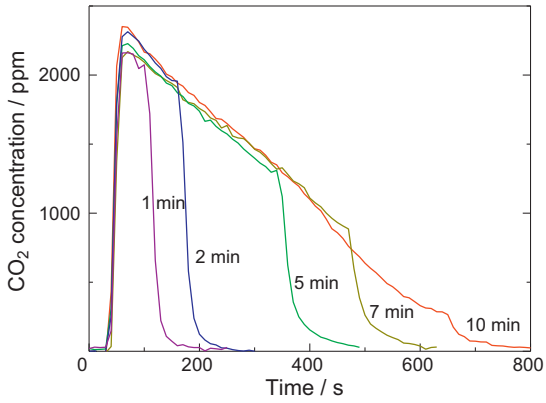


**Fig. 3.** Profiles of formed $CO_2$ during partial reduction of 5 wt%Pd/$SiO_2$ in a flow of 0.45%CO/He at 400 °C.

other factors for the low temperature activity. The reduction of the support in a flow of CO may be the key for the mismatch. In order to simplify the activity-controlling factors, the effect of Pd oxidation state is examined using model Pd/$SiO_2$ in the next section, and the contribution of the lattice oxygen of the supports is examined in Section 3.4.

### 3.3. Effect of oxidation number of PdOx/$SiO_2$

The effect of oxidation number of supported Pd on catalytic activity was evaluated using 5 wt% Pd/$SiO_2$ as a model catalyst having minimum interaction between Pd and support. The average oxidation number of Pd was controlled by partial reduction of Pd/$SiO_2$ in a flow of 0.45% CO/He at 400 °C for prescribed time. After the oxidation in a flow of 10% $O_2$/He at 400 °C for 10 min, 0.45%CO/He was fed to Pd/$SiO_2$ at 400 °C, and the profiles of $CO_2$ formation were measured, as shown in Fig. 3. After 10 min reduction by CO, the effluent $CO_2$ concentration was almost zero, and the integrated amount of $CO_2$ was equivalent to PdO, indicating complete reduction of PdO to Pd as in the following equation.

$$CO + PdO \rightarrow CO_2 + Pd$$

When the CO feed was cut-off for less than 10 min, the supported Pd was partially reduced. From the amount of produced $CO_2$, average oxidation numbers of Pd ($x$ in PdO$x$) were estimated. The $x$ in PdO$x$ was varied with the reduction time, and those were 1.0 (0 min), 0.80 (1 min), 0.65 (2 min), 0.31 (5 min), 0.24 (7 min) and 0.0 (10 min), respectively.

Fig. 4 shows XRD patterns of the series of obtained Pd/$SiO_2$. Pd/$SiO_2$ after the oxidation in $O_2$ (0 min) showed the diffraction lines of PdO at $2\theta = 33.9°$ and 42.0°. As the reduction time increased, the diffraction lines of PdO decreased, while that of metallic Pd increased. After the reduction by CO for 10 min, the lines of PdO completely disappeared and the line of metallic Pd clearly observed. From the Scherrer equation, the particle diameter of PdO was estimated as 14.8 nm. The particle diameter of Pd was estimated as 21.1 nm. The negligible effect of these pretreatments on the particle diameter of Pd species was also confirmed by TEM as shown in Fig. 5. The particle diameter of PdO on 5 wt%Pd/$SiO_2$ was estimated as $9.2 \pm 3.0$ nm after the oxidation at 400 °C in a flow of 10%$O_2$/He for 10 min. After the reduction in 0.45%CO/He at 400 °C, the diameter of Pd species was estimated as $8.6 \pm 2.2$ nm after 5 min, and $10.2 \pm 2.7$ nm after 10 min. Although the particles sizes slightly increased by the full reduction, the size change was not significant. The larger apparent particle size estimated by XRD may be due to the less sensitivity to smaller crystals. It was confirmed that the partial reduction by CO successfully prepared PdO$x$/$SiO_2$ catalysts

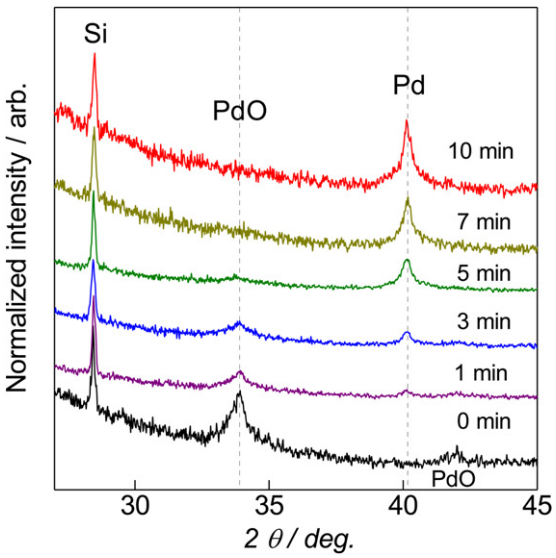


**Fig. 4.** XRD patterns of 5 wt%PdO$x$/$SiO_2$ after partial reduction by CO. The intensity of the lines was normalized using Si(1 1 1) at $2\theta = 28.45°$ as an internal standard.

with the $x$ value from 0.0 to 1.0 without significant sintering of Pd species.

By using the series of Pd/$SiO_2$, the effect of the average oxidation number of Pd on the catalytic activity for CO oxidation was investigated. Fig. 6 shows the relationship between the CO oxidation activity at 140 °C and the average oxidation number of Pd. Since the oxidation number of supported Pd varied during the CO flow reaction, the initial rate of CO oxidation was compared. Clearly, the CO oxidation activity steeply decreased with the increase in the $x$ in PdO$x$. The deactivation is not due to the sintering of Pd species, because the changes in particle size are negligible as indicated by XRD and TEM. The results indicate that the metallic Pd is the active species for CO oxidation over Pd/$SiO_2$.

Although there have been still some discussions on the active oxidation state of Pd during the oxidation reactions, metallic Pd is generally assigned as the active species in the case of CO oxidation at low temperatures [33,38,39]. This is reasonable because the mobility of lattice oxygen in PdO$x$ matrix is low at lower temperatures and the surface oxygen inhibits the adsorption of CO. Without the assistance of supports, it is reasonable to assign metallic Pd as the active species for catalytic oxidation at low temperatures, and the CO oxidation proceeds a typical Langmuir–Hinshelwood mechanism.

### 3.4. Contribution of supports

Fig. 7 shows the profile of $CO_2$ formation during CO–$O_2$ pulse reaction without gaseous $O_2$. The amount of formed $CO_2$ was in the order of Pd/$CeO_2$ > Pd/$TiO_2$ > Pd/$Al_2O_3$, which is the same order with the catalytic activity of CO oxidation. The profile was reproducible for several times. Table 3 summarized the amount of formed $CO_2$

**Table 3**
Amount of formed $CO_2$ during anaerobic CO pulse reaction.

| Catalyst | From $O_2$ to CO | | From CO to $O_2$ | |
|---|---|---|---|---|
| | $CO_2$ (mmol $g^{-1}$) | $CO_2$/Pd molar ratio | $CO_2$ (mmol $g^{-1}$) | $CO_2$/Pd molar ratio |
| Pd/$CeO_2$ | 2.1 | 22 | 0.066 | 0.71 |
| Pd/$TiO_2$ | 0.75 | 8.0 | 0.063 | 0.67 |
| Pd/$Al_2O_3$ | 0.059 | 0.63 | 0.053 | 0.56 |
| Pd/$ZrO_2$ | 0.028 | 0.30 | 0.023 | 0.25 |
| Pd/$SiO_2$ | 0.044 | 0.46 | 0.042 | 0.45 |

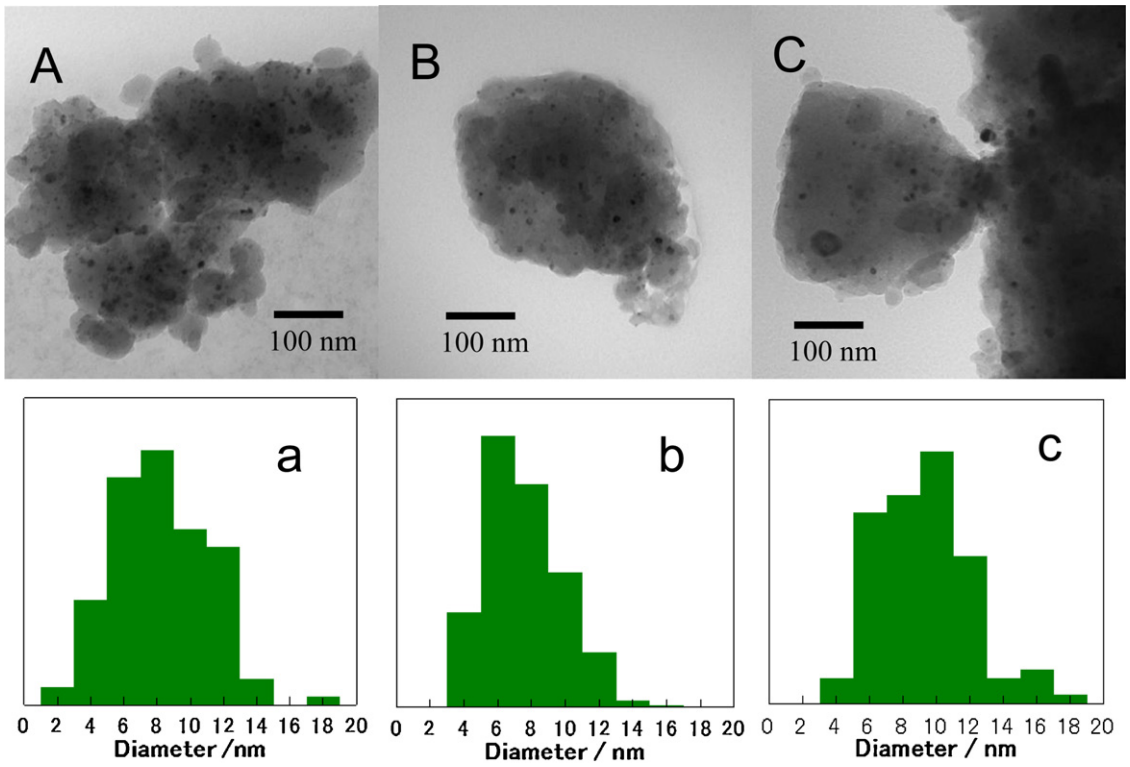


**Fig. 5.** TEM images (A–C) and distributions of Pd particle diameter (a–c) of 5 wt%Pd/$SiO_2$ pretreated at 400 °C in a flow of (A and a) 10%$O_2$/He for 10 min, (B and b) 0.45%CO/He for 5 min, and (C and c) 0.45%CO/He for 10 min.

during anaerobic CO pulse reaction. The $CO_2$/Pd ratios were below unity in the case of Pd/$Al_2O_3$, Pd/$ZrO_2$, and Pd/$SiO_2$, while those exceeded unity in the case of Pd/$CeO_2$ and Pd/$TiO_2$. It is clear that the lattice oxygen of supports contributed to the formation of $CO_2$ with the role of oxygen storage property, which is well known nature of $CeO_2$ [54–56]. Pd/$TiO_2$ also showed oxygen storage property, although the $CO_2$/Pd ratio was lower than Pd/$CeO_2$. A good agreement of oxygen storage property and the catalytic activity of CO oxidation suggest the oxygen storage property of supports is another factor for the low-temperature CO oxidation.

The order of the reaction with respect to CO and $O_2$ were examined as shown in Fig. 8, and the results are summarized in Table 4. Because of the different light-off temperature on each catalyst, the reaction temperature was optimized for each catalyst. The data of Pd/$SiO_2$ were not plotted because of far lower reaction rates compared to the other catalysts. The reaction order on Pd/$Al_2O_3$ was around 0.5 with respect to $O_2$, suggesting typical Langmuir–Hinshelwood mechanism involving cleavage of oxygen molecule on the metal surface. The negative order to CO indicates self-poisoning of Pd surface by strongly adsorbed CO at lower temperatures. Pd/$ZrO_2$ and Pd/$SiO_2$ showed the similar trend. On the other hand, Pd/$CeO_2$ and Pd/$TiO_2$ showed the different order of the reaction, i.e., the positive order with respect to CO and the lower order to $O_2$. The positive order of the reaction to CO suggests that

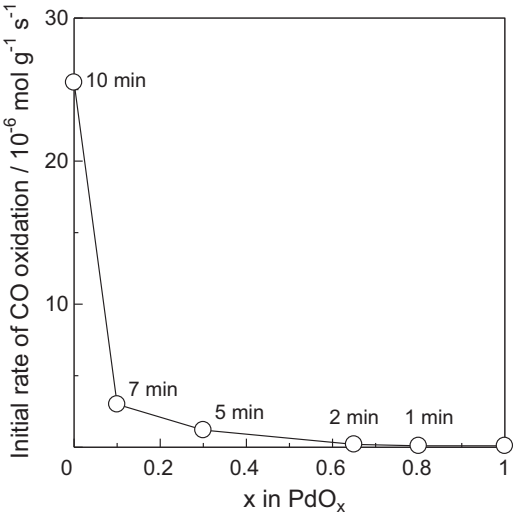


**Fig. 6.** Initial reaction rate of CO oxidation at 140 °C over 5 wt%PdO*x*/$SiO_2$ having various average oxidation number of PdO*x*.

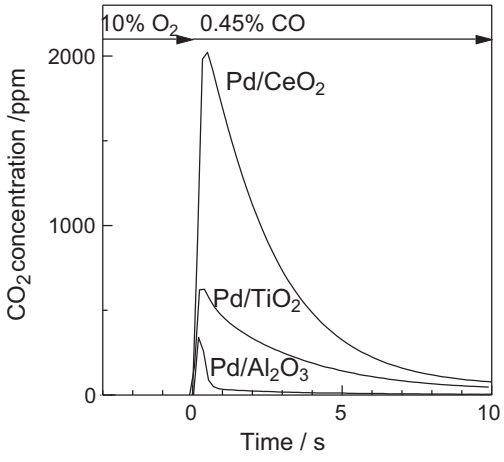


**Fig. 7.** Profiles of $CO_2$ formation during CO pulse reaction without $O_2$ at 100 °C. The catalysts were at first treated in a flow of 0.45% CO/He for 5 min, switched to a flow of 10% $O_2$/He for 10 min, and again switched to a flow of 0.45% CO/He for 10 min. The amounts of produced $CO_2$ during $O_2$ pulse and CO pulses were summarized in Table 3.

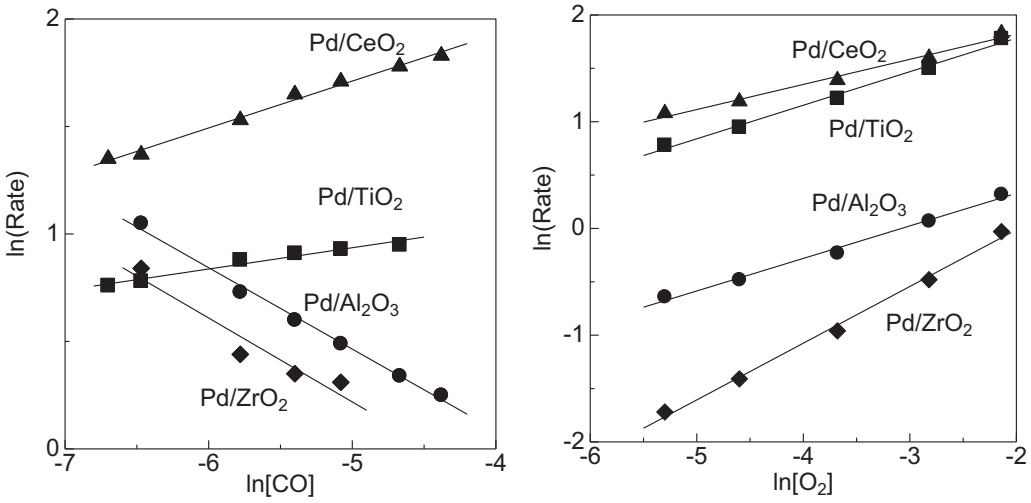


**Fig. 8.** Dependence of the reaction rate on the partial pressure of CO (left) and $O_2$ (right) over Pd supported catalysts. The reaction temperatures on each catalyst were indicated in Table 4.

the oxidation of CO proceeds regardless of the strongly adsorbed CO on Pd. The order with respect to $O_2$ was nearly zero on $Pd/CeO_2$ and $Pd/TiO_2$, suggesting Mars-van Krevelen mechanism [57] with the contribution of $CeO_2$ and $TiO_2$ supports as an oxygen supply.

Fig. 9 shows IR spectra of adsorbed CO on $Pd/Al_2O_3$ and $Pd/CeO_2$ at various temperatures. The spectra at 27 °C shows bimodal bands at 2175 and 2090 $cm^{-1}$ assignable to the linearly bonded CO on $Pd^{2+}$ and $Pd^{+}$, a sharp band at 2090 $cm^{-1}$ assignable to linear CO on $Pd^0$ and 1950 $cm^{-1}$ assignable to bridge-bonded CO on $Pd^0$, respectively [29,35,58–64]. It should be noted that the adsorption of CO on surface of the supports can be neglected because no CO band was observed on pure support material under the present conditions. With the increase in the reaction temperature, the bands assignable to adsorbed CO gradually decreased, instead, the $CO_2$ band at 2360 $cm^{-1}$ increased [58,65], indicating the surface conversion of CO into $CO_2$. Actually, the concentration of $CO_2$ in the effluent gas also increased with the increase in the temperature. Although the bands of linear CO adsorbed on both oxidized Pd and metallic Pd are overlapped, the intensity of the band at 2090 $cm^{-1}$ was used as a tentative measure of the coverage of CO on Pd surface. Assuming that the CO coverage on Pd surface is 100% at room temperature, the surface coverage with CO and the catalytic activity determined from the effluent gas concentration from in situ IR cell are compared.

Fig. 10 shows the dependence of the catalytic activity on the CO coverage. The conversion of CO over $Pd/Al_2O_3$ started when the CO coverage became below 0.5, while $Pd/CeO_2$ and $Pd/TiO_2$ showed the activity even when the surface is almost fully covered by CO. The oxygen storage capacities measured at 100 °C were 2.1 mmol $g^{-1}$ for $Pd/CeO_2$ and 0.75 mmol $g^{-1}$ for $Pd/TiO_2$, respectively. Considering the oxygen release and storage capacities of $CeO_2$ and $TiO_2$, the activity of $Pd/CeO_2$ and $Pd/TiO_2$ at very high CO coverage is due to the contribution of oxygen supply from the support. Consequently, the higher activity of $Pd/CeO_2$ and $Pd/TiO_2$ can be attributed to both the higher reducibility of Pd and the

**Table 4**
Order of the CO oxidation over Pd supported catalysts with respect to CO and $O_2$.

| Catalyst | Reaction order with respect to CO | | Reaction order with respect to $O_2$ | |
|---|---|---|---|---|
| | Temperature (°C) | Order | Temperature (°C) | Order |
| $Pd/CeO_2$ | 60 | 0.22 | 60 | 0.24 |
| $Pd/TiO_2$ | 80 | 0.10 | 100 | 0.31 |
| $Pd/Al_2O_3$ | 120 | −0.38 | 100 | 0.53 |
| $Pd/ZrO_2$ | 140 | −0.40 | 140 | 0.32 |
| $Pd/SiO_2$[a] | 100 | −0.33 | 100 | 0.56 |

[a] Catalyst weight: 100 mg.

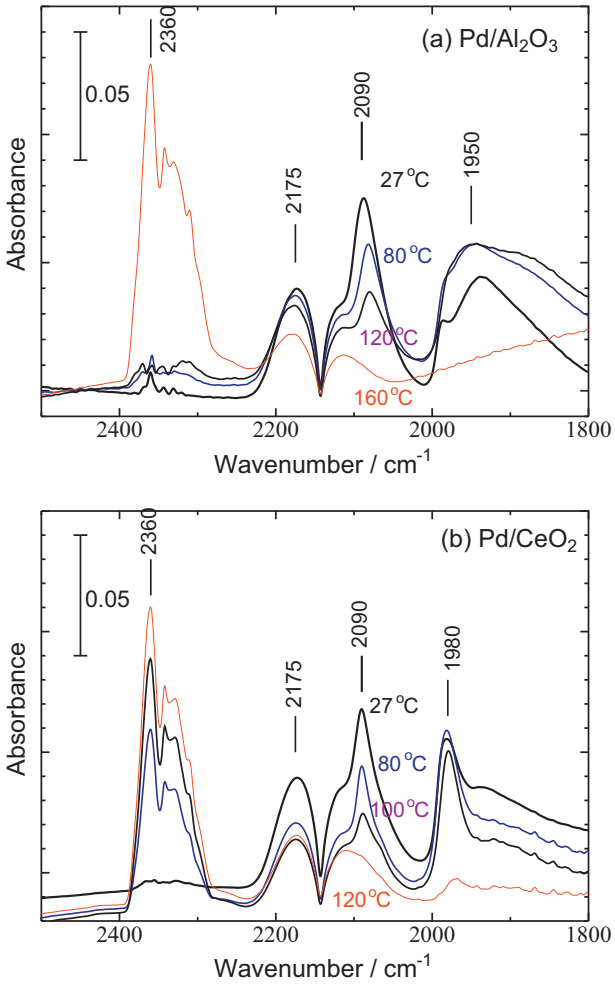


**Fig. 9.** IR spectra of adsorbed CO on $Pd/Al_2O_3$ at various temperatures.

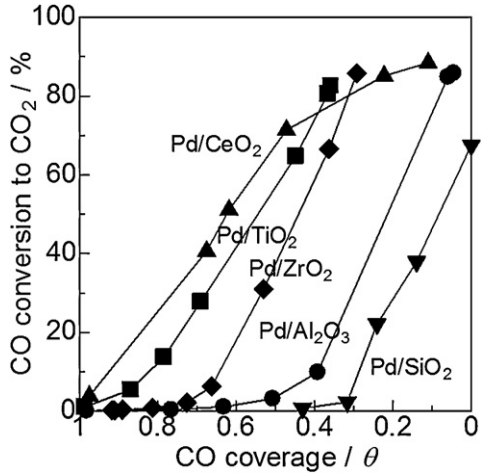


**Fig. 10.** Relationship between CO coverage and conversion of CO to $CO_2$ over supported Pd catalysts (Pd 1 wt%) in a flow of 0.45%CO/10%$O_2$/He from room temperature to 160 °C.

contribution of lattice oxygen of supports having sufficient oxygen storage capacity.

## 4. Conclusions

The present study clarified the contribution of two controlling factors for the low temperature oxidation of CO on supported Pd catalysts. One is the reducibility of PdO to Pd, and another is the contribution of lattice oxygen of supports having sufficient oxygen release and storage property. Although the competitive adsorption of CO and $O_2$ on Pd surface suppresses CO oxidation on $Pd/Al_2O_3$ at lower temperatures, the oxygen activation on the support improves catalytic cycles on $Pd/CeO_2$ and $Pd/TiO_2$.

## Acknowledgements

The authors greatly appreciate to Dr. Yuta Yamamoto and Dr. Shigeo Arai in Ecotopia Science Instituite, Nagoya University for their helpful discussions and suggestions on TEM measurements. This work was partly supported by JSPS KAKENHI Grant Number 23360354, MEXT program "Elements Strategy Initiative to Form Core Research Center" from the Ministry of Education, Culture, Sports, Science and Technology, Japan.

## References

[1] R.F. Hicks, H. Qi, M.L. Young, R.G. Lee, Journal of Catalysis 122 (1990) 295–306.
[2] H. Maeda, Y. Kinoshita, K.R. Reddy, K. Muto, S. Komai, N. Katada, M. Niwa, Applied Catalysis A-General 163 (1997) 59.
[3] D. Ciuparu, L. Pfefferle, Applied Catalysis A-General 209 (2001) 415–428.
[4] K. Eguchi, H. Arai, Applied Catalysis A-General 222 (2001) 359–367.
[5] W. Lin, Y.X. Zhua, N.Z. Wu, Y.C. Xie, I. Murwani, E. Kemnitz, Applied Catalysis B: Environmental 50 (2004) 59–66.
[6] K. Okumura, E. Shinohara, M. Niwa, Catalysis Today 117 (2006) 577–583.
[7] V. Ferrer, A. Moronta, J. Sánchez, R. Solano, S. Bernal, D. Finol, Catalysis Today 107–108 (2005) 487–492.
[8] H. Yoshida, T. Nakajima, Y. Yazawa, T. Hattori, Applied Catalysis B: Environmental 71 (2007) 70–79.
[9] X. Wang, Y. Guo, G. Lu, Y. Hu, L. Jiang, Y. Guo, Z. Zhang, Catalysis Today 126 (2007) 369–374.
[10] B. Stasinska, A. Machocki, K. Antoniak, M. Rotko, J.L. Figueiredo, F. Gonçalves, Catalysis Today 137 (2008) 329–334.
[11] S. Specchia, P. Palmisano, E. Finocchio, M.A.L. Vargas, G. Busca, Applied Catalysis B: Environmental 92 (2009) 285–293.
[12] P. Castellazzi, G. Groppi, P. Forzatti, E. Finocchio, G. Busca, Journal of Catalysis 275 (2010) 218–227.
[13] A.D. Mayernick, M.J. Janik, Journal of Catalysis 278 (2011) 16–25.
[14] R. Burch, P.K. Loader, F.J. Urbano, Catalysis Today 27 (1996) 243–248.
[15] D.P. Chzhu, P.G. Tsyrul'nikov, G.N. Kryukova, V.F. Borbat, E.N. Kudrya, M.D. Smolikov, A.V. Bubnov, Kinetics and Catalysis 4 (2004) 406–413.
[16] J.-M. Giraudon, A. Elhachimi, F. Wyrwalski, S. Siffert, A. Aboukaïs, J.-F. Lamonier, G. Leclercq, Applied Catalysis B: Environmental 75 (2007) 157–166.
[17] K.B. Kim, M.K. Kim, Y.H. Kim, K.S. Song, E.D. Park, Research on Chemical Intermediates 36 (2010) 603–611.
[18] A. Satsuma, R. Sato, K. Osaki, K. Shimizu, Catalysis Today 185 (2012) 61–65.
[19] M. Fernández-García, A. Martínez-Arias, A. Iglesias-Juez, A.B. Hungría, J.A. Anderson, J.C. Conesa, J. Soria, Applied Catalysis B: Environmental 31 (2001) 39–50.
[20] M. Fernández-García, A. Martínez-Arias, A. Iglesias-Juez, A.B. Hungría, J.A. Anderson, J.C. Conesa, J. Soria, Applied Catalysis B: Environmental 31 (2001) 51–60.
[21] J.A. Wang, L.F. Chen, M.A. Valenzuela, A. Montoya, J. Salmonesb, P.D. Angel, Applied Surface Science 230 (2004) 34–43.
[22] H. Zhu, Z. Qin, W. Shan, W. Shen, J. Wang, Journal of Catalysis 225 (2004) 267–277.
[23] H. Zhu, Z. Qin, W. Shan, W. Shen, J. Wang, Journal of Catalysis 233 (2005) 41–50.
[24] G.P. Osorio, S.F. Moyado, V. Petranoxskii, A. Simakov, Catalysis Letters 110 (2006) 53–60.
[25] J.-Y. Luo, M. Meng, X. Li, X.-G. Li, Y.-Q. Zha, T.-D. Hu, Y.-N. Xie, J. Zhang, Journal of Catalysis 254 (2008) 310–324.
[26] C.-W. Tang, M.-C. Kuo, C.-J. Lin, C.-B. Wang, S.-H. Chien, Catalysis Today 131 (2008) 520–525.
[27] A.I. Boronin, E.M. Slavinskaya, I.G. Danilova, R.V. Gulyaev, Y.I. Amosov, P.A. Kuznetsov, I.A. Polukhina, S.V. Koscheev, V.I. Zaikovskii, A.S. Noskov, Catalysis Today 144 (2009) 201–211.
[28] B. Wang, D. Weng, X. Wu, J. Fan, Catalysis Today 153 (2010) 111–117.
[29] B. Wang, D. Weng, X. Wu, R. Ran, Applied Surface Science 257 (2011) 3878–3883.
[30] A.S. Ivanova, E.M. Slavinskaya, R.V. Gulyaev, V.I. Zaikovskii, O.A. Stonkus, I.G. Danilova, L.M. Plyasova, I.A. Polukhina, A.I. Boronin, Applied Catalysis B: Environmental 97 (2010) 57–71.
[31] S. Colussi, A. Trovarelli, E. Vesselli, A. Baraldi, G. Comelli, G. Groppi, J. Llorca, Applied Catalysis A-General 390 (2010) 1–10.
[32] L. Liu, F. Zhou, L. Wang, X. Qi, F. Shi, Y. Deng, Journal of Catalysis 274 (2010) 1–10.
[33] R.V. Gulyaev, A.I. Stadnichenko, E.M. Slavinskaya, A.S. Ivanova, S.V. Koscheev, A.I. Boronin, Applied Catalysis A-General 439–440 (2012) 41–50.
[34] Y. Nishihata, J. Mizuki, T. Akao, H. Tanaka, M. Uenishi, M. Kimura, T. Okamoto, N. Hamada, Nature 418 (2002) 164–167.
[35] S. Specchia, E. Finocchio, G. Busc, P. Palmisano, V. Specchia, Journal of Catalysis 263 (2009) 134–145.
[36] S. Specchia, E. Finocchio, G. Busca, G. Saracco, V. Specchia, Catalysis Today 143 (2009) 86–93.
[37] T. Schalow, B. Brandt, M. Laurin, S. Schauermann, S. Guimond, H. Kuhlenbeck, J. Libuda, H.-J. Freund, Surface Science 600 (2006) 2528–2542.
[38] M. Lyubovsky, L. Pfefferle, Catalysis Today 47 (1999) 29–44.
[39] L.-Y. Jin, J.-Q. Lu, X.-S. Liu, K. Qian, M.-F. Luo, Catalysis Letters 128 (2009) 379–384.
[40] C. Bozo, N. Guilhaume, J.-M. Herrmanny, Journal of Catalysis 203 (2001) 393–406.
[41] T. Jin, T. Okuhara, G.J. Mains, J.M. White, Journal of Physical Chemistry 91 (1987) 3310–3315.
[42] G.S. Zafiris, R.J. Gorte, Journal of Catalysis 139 (1993) 561–567.
[43] H. Cordatos, R.J. Gorte, Journal of Catalysis 159 (1996) 112–118.
[44] A. Tömcrona, M. Skoglundh, P. Thormählen, E. Fridell, E. Jobson, Applied Catalysis B: Environmental 14 (1997) 131–146.
[45] A. Martínez-Arias, M. Fernández-García, A. Iglesias-Juez, A.B. Hungría, J.A. Anderson, J.C. Conesa, J. Soria, Applied Catalysis B: Environmental 31 (2001) 39–50.
[46] S. Yang, W. Zhu, Z. Jiang, Z. Chen, J. Wang, Applied Surface Science 252 (2006) 8499–8505.
[47] F. Liang, H. Zhu, Z. Qin, G. Wang, J. Wang, Catalysis Communications 10 (2009) 737–740.
[48] K. Nakagawa, Y. Murata, M. Kishida, M. Adachim, M. Hiro, K. Susa, Materials Chemistry and Physics 104 (2007) 30–39.
[49] T. Tanabe, Y. Nagai, T. Hirabayashi, N. Takagi, K. Dohmae, N. Takahashi, S. Matsumoto, H. Shinjoh, J.N. Kondo, J.C. Schouten, H.H. Brongersma, Applied Catalysis A-General 370 (2009) 108–113.
[50] K. Shimizu, Y. Saito, T. Nobukawa, N. Miyoshi, A. Satsuma, Catalysis Today 139 (2008) 24–28.
[51] K. Shimizu, Y. Saito, T. Nobukawa, A. Satsuma, Topics in Catalysis 53 (2010) 584–590.
[52] A. Satsuma, K. Shimizu, Progress in Energy and Combustion Science 29 (2003) 71–84.
[53] S. Ojala, N. Bion, A. Baylet, M. Tarighi, R.L. Keiski, D. Duprez, Applied Catalysis B: Environmental 108–109 (2011) 22–31.
[54] J. Kašpar, P. Fornasiero, M. Graziani, Catalysis Today 50 (1999) 285–298.
[55] S. Matsumoto, Catalysis Today 90 (2004) 183–190.
[56] M. Sugiura, M. Ozawa, A. Suda, T. Suzuki, T. Kanazawa, Bulletin of the Chemical Society of Japan 78 (2005) 752–767.
[57] M.A. Vannice, Catalysis Today 123 (2007) 18–22.
[58] Y.-X. Jiang, N. Ding, S.-G. Sun, Journal of Electroanalytical Chemistry 563 (2004) 15–21.
[59] C. Mondelli, D. Ferri, J.-D. Grunwaldt, F. Krumeich, S. Mangold, R. Psaro, A. Baiker, Journal of Catalysis 252 (2007) 77–87.

[60] M. Skotak, Z. Karpiński, W. Juszczyk, J. Pielaszek, L. Kępiński, D.V. Kazachkin, V.I. Kovalchuk, J.L. d'Itri, Journal of Catalysis 227 (2004) 11–25.
[61] K. Nakao, O. Watanabe, T. Sasaki, S. Ito, K. Tomishige, K. Kunimori, Surface Science 601 (2007) 3796–3800.
[62] G. Busca, E. Finocchio, V.S. Escribano, Applied Catalysis B: Environmental 113–114 (2012) 172–179.
[63] E. Groppo, G. Agostini, A. Piovano, N.B. Muddada, G. Leofanti, R. Pellegrini, G. Portale, A. Longo, C. Lamberti, Journal of Catalysis 287 (2012) 44–54.
[64] Y. Ji, G. Liu, W. Li, W. Xiao, Journal of Molecular Catalysis A: Chemical 314 (2009) 63–70.
[65] R. Di Monte, J. Kaspar, P. Fornasiero, M. Graziani, C. Paze, G. Gubitosa, Inorganica Chimica Acta 334 (2002) 318–326.